SciMedCentral

Journal of Radiology & Radiation therapy

Case Report

Distinctive Energy Profile of Water-Soluble, Thiolate-Protected Gold Nanoparticles as Potential Molecular Marker for Vulnerable Plaque Detection with XFCT Imaging

Raiyan T. Zaman[1]*, Don Vernekhol[2], and Lei Xing[2]

[1]*Department of Radiology, Harvard Medical School, USA*
[2]*Department of Radiation Oncology, Division of Medical Physics, Stanford University School of Medicine, USA*

***Corresponding author**
Raiyan T. Zaman, PhD, MSEE, Assistant Professor, Department of Radiology, Harvard Medical School, Assistant Investigator, Gordon Center for Medical Imaging Massachusetts General Hospital, 149, 13th Street, Charlestown, Boston, MA 02129, Tel: (617) 643-9610 (O); (512) 294-7327 (C); Email: rzaman@mgh.harvard.edu

Submitted: 21 September 2020
Accepted: 10 October 2020
Published: 12 October 2020
ISSN: 2333-7095

Abstract

Purpose: X-ray CT plays a pivotal role in diagnostic imaging, radiotherapy, and its indispensable contribution to preclinical small animal imaging research. This study characterizes a distinctive energy spectrum of a novel 3-mercaptobenzoic-acid (3MBA)-protected-144-atoms gold-nanoparticles (3MBA-Au-144-NPs) after X-ray excitation and detects vulnerable atherosclerotic plaques non-invasively using this novel contrast agent in mice carotid arteries for the first time to the best of our knowledge.

Methods: We designed a four-chamber heart apex model using a 3D-printer and filled with four different concentrations of 3MBA-Au-144-NPs. The X-ray system was equipped with a pencil beam collimator, which was calibrated using a 1x1 in^2 large radiochromic film. The tube was operated at 320 kVp with 12.5 mA current and multiple filtration options were available for the X-ray excitation source. The resulting pencil beam had a 3.2 mm diameter. The four-chamber apex was translated and rotated relative to the stationary pencil beam. Each sample chamber was irradiated for 2-minutes and emitted fluorescent X-rays from the excited 3MBA-Au-144-NPs were collected with CdTe and Silicon Drift (SD) detectors for 15 seconds. The spectra were used for L-shell XRF peak isolation and sonogram generation of this novel 3MBA-Au-144-NPs. The distribution and concentration of 3MBA-Au-144-NPs were reconstructed with an alternative maximum likelihood expectation maximization algorithm. For *in vivo* detection of unstable plaques, we developed atherosclerotic mice model after feeding them 1% high cholesterol diet (HCD) for four weeks before diabetic was induced by intraperitoneal injection of streptozotocin (STZ) to accelerate the plaque progression. Two weeks after the diabetic induction, surgically left carotid artery was ligated. Two weeks after the surgical ligation, a 250 µL of 3MBA-Au-144-NPs was IV injected after 6 hours of fasting. One hour after injection, the mice were imaged non-invasively with a cone-beam micro-CT system.

Results: Two distinctive L-shell energy peaks were observed at 10 KeV and 11.13 KeV for 3MBA-Au-144-NPs in the energy spectrum of the SD detector. K-shell fluorescence events vanished in the Compton scatter and characteristic background of the tungsten source due to the lead shielding for the SD and CdTe detectors. There is a space missing at 12.5 KeV. The signal intensity varied with different 3MBA-Au-144-NPs concentration of 5%, 10%, 20%, and 100%. The X-ray fluorescence (XRF) intensity showed a highly linear response (R^2=0.999) with respect to different concentrations of 3MBA-Au-144-NPs. High XRF signal was detected in the left carotid artery at 2 mm below the ligation and in aortic arch. Non-ligated right carotid artery (negative control) showed no such signal.

Conclusion: These distinct energy spectra in the L-shell fluorescent energies render 3MBA-Au-144-NPs as a viable contrast agent for future *in vivo* XFCT imaging.

INTRODUCTION

X-ray based computed tomography (CT) plays a pivotal role in diagnostic imaging, image guided interventions, treatment planning of various diseases. Although CT provides millimeter resolution for anatomical imaging, it lacks the ability to image processes at the molecular level. When dealing cardiovascular diseases, it is difficult to image atherosclerotic plaques within the coronary artery due to its small size, motion, and obscuring signal from surrounding myocytes even with dynamic contrast-enhanced CT while measuring physiological properties. However, X-ray fluorescence CT (XFCT) is an intriguing alternative on the basis of physical principle to detect characteristic X-ray emissions from high atomic-number (Z) elements when exposed to X-ray beam [1,2]. Following photoelectric absorption, a vacancy in the K shell is subsequently filled by an electron from L or M shells, and the energy difference between these shells is released as either an Auger electron or a characteristic K-shell X-ray (i.e., XRF). In this study, we have used novel water-soluble thiolate-protected gold nanoparticles called 3-mercaptobenzoic-acid (3MBA)-protected-144-atoms gold-nanoparticles (3MBA-Au-144-NPs) [3] made of element with an atomic number Z ≥47 to characterize the distinctive energy spectrum after X-ray excitation for the first time to the best of our knowledge.

With the goal of utilizing the XFCT signals for cardiovascular applications, here we investigated an imaging method to directly monitor the spatial distribution of the 3MBA-Au-144-NPs using XFCT to identify the location of vulnerable plaques in carotid arteries by detecting characteristics X-ray (XRF photons) or

Augur electrons from 3MBA-Au-144-NPs through photoelectric process. The XRF photons can be imaged with energy-resolving X-ray photon counting detectors [4-6]. This will provide a means of detecting quantitative change in distribution and concentration of 3MBA-Au-144-NPs. We present the instrumentation development with a heart apex phantom validation followed by *in vivo* imaging of atherosclerotic plaques in mice carotid arteries in conjunction with 3MBA-Au-144-NPs with a cone-beam micro-CT imaging system.

In this study, we have demonstrated two distinctive L-shell energy peaks specific to 3MBA-Au-144-NPs contrast agent recently developed in Dr. Kornberg's laboratory. Based on XRF peaks in the spectra of the processed sonogram for each chamber of 3D printed apex model showed highly linear response (R^2=0.999) with respect to different concentrations of 3MBA-Au-144-NPs and their signal intensity. We have also detected strong XRF signal in the close vicinity of the left carotid arterial ligation in the mice atherosclerotic model that highlights the presence of unstable plaques infiltrated with macrophage with micro-CT imaging system in conjunction of 3MBA-Au-144-NPs.

MATERIALS AND METHODS

MBA-Au-144-NPs synthesis

3MBA protected gold nanoparticles (AuNPs) were synthesize as described before [3]. Briefly, methanolic solutions of 3-MBA (84 mM) and HAuCl4 (28 mM) were mixed in 7:1 molar ratio. The mixture was diluted 3.5-fold in water, pH was adjusted to 13 by addition of about 100 mM NaOH, and mixture was equilibrated overnight. A final solution of 2.5 mM 3-MBA, 0.36 mM HAuCl4, and 27% (v/v) methanol was reduced with 2 mM NaHB4. Reaction proceeded on rocking platform for 4.5 hours at room temperature. Au144 nanoparticles were recovered by precipitation with 100 mM NaCl and centrifugation. After a final wash in 75% methanol, the pellet was dried in air overnight and suspended in water.

Phantom preparation

We designed a four-chamber heart apex model and its holder using a 3D-printer (Figure 1A). Each chamber had the dimension of 3 mm, which is within the human coronary artery diameter (1.9-4.5 mm), and 10 mm height. Chambers were filled with 0.1 ml of 17 mg/mL 3MBA-Au-144-NPs and 0, 0.05, 0.1, and 0.2 ml of water to make the final 3MBA-Au-144- concentrations to be 17.0, 3.4, 1.7, and 0.85 mg/ml, respectively (Figure 1B).

XFCT system setup

The schematic diagram of the experimental setup is illustrated in Figure 2A. The X-ray system was equipped with a pencil beam collimator, which was calibrated using a 1x1 in^2 large radiochromic film. The mechanism of X-ray fluorescence (XRF) emission from L-shell electrons is shown in Figure 2B. The X-ray tube was operated at 320 kVp with 12.5 mA current and multiple filtration options were available for the X-ray excitation source (PXi, Precision X-Ray, CT, USA) (Figure 3A). The resulting pencil beam diameter was 3.2 mm. The detectors and sample chambers were shielded elaborately (Figure 3B) with lead to effectively suppress scatter background from the X-ray tube and

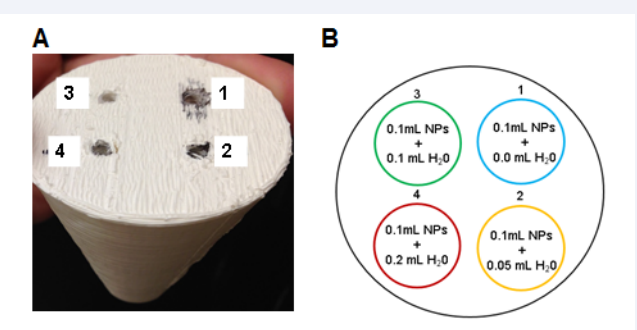

Figure 1 (A) Photograph of the four-chamber heart apex model filled with different concentrations of 3MBA-Au-144-NPs.Schematic illustration of the (B) apex model with various concentrations of the 3MBA-Au-144-NPs within the four chambers.

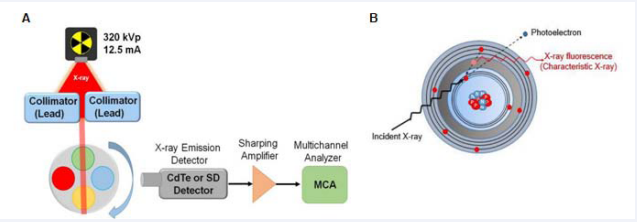

Figure 2 (A) Schematic illustration of the experimental setup including the filtered X-ray source, the heart apex model with different concentrations of 3MBA-Au-144-NPs, and the CdTe or SD detector. (B) Mechanism of the X-ray fluorescence (XRF) photon emission from L-shell electrons.

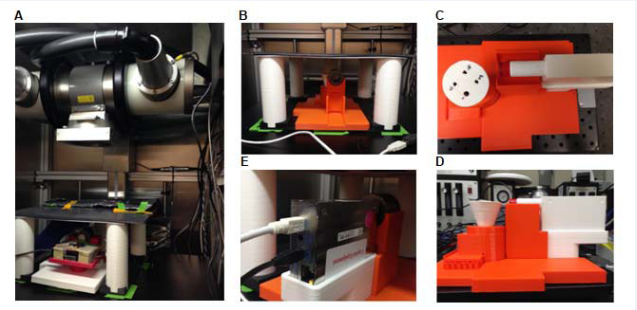

Figure 3 Photograph of the experimental set-up with (A) X-RAD 320 from PXi Precision X-ray with CdTe detector, (B) collimator with lead shielding, the heart apex model (C) a top, (D) a side view, and (E) SD detector.

provide a high sensitivity for the measurement. The XFCT system setup with a 3D printed holder and mock detectors were shown in Figure 3C-3D. Each sample chambers with the NPs was irradiated for 2 minutes before detecting the X-ray photons from 3MBA-Au-144-NPs with a thermoelectrically cooled cadmium telluride (CdTe) (Figure 3A) and Silicon Drift (SD) detectors (Figure 3E).

The heart apex model was set up in a rotating motion at precise steps using a computer-controlled motion stage (Velmex Inc., Bloomfield, NY), while the X-ray source and the detectors were kept stationary. A single slice of measurements was acquired by translating the heart apex model 30× at 1.5 mm

increments. To cover one complete rotation of 360° degree it took 31×. The emitted XRF photons from the pencil beam illuminated narrow volume were collected using CdTe (X-123CdTe, Amptek Inc., Bedford, MA) detector. The x-ray detector module included a preamplifier with pile-up rejection, a digital pulse processor and a multichannel analyzer (MCA) (PX4, Amptek Inc., Bedford, MA). The detector and motion stage were operated by a custom written C++ program from a computer. The detectors system was placed at a 90° angle to the incident X-ray beam to minimize the number of unwanted scattered photons entering the detectors. To shield the X-ray detectors from X-rays coming from outside the field of view, a thick lead shield was built to cover the sensitive elements. A second SDD X-ray detector SD (1-2-3 X-Ray Spectrometer, Amp TeK) was placed behind the apex heart model along the beam direction to provide transmission measurements.

Sinogram generation from spectrum analysis

XFCT raw data consisted of a series of spectra with corresponding beam position. The XRF peaks in the spectra were processed into a sonogram for each chamber of Apex model consisted of different concentration of 3MBA-Au-144-NPs and reconstructed with 25 iterations of maximum-likelihood expectation maximization (MLEM) algorithm. The spectra included fluorescence peaks from 3MBA-Au-144-NPs as well as the background due to scattered photons. Although, L-shell XRF has low-penetration, we focused on acquiring both L-shell and K-shell XRF peaks. The spectrum measured for each beam position includes the L-shell and K-shell XRF peaks from 3MBA-Au-144-NPs superimposed on a broad background of scattered photons.

Mice atherosclerotic model development

Mice experiments were conducted according to a protocol approved by the Administrative Panel on Laboratory Animal Care at the Massachusetts General Hospital (APLAC #2019N000104). Macrophage-rich atherosclerotic lesions were created in the left carotid arteries of diabetic, hyperlipidemic FVB/NJ mice, as studied extensively by our laboratory [7-10]. In brief, 8-week-old male mice (n=5) were started with normal chow immediate after arrival at the MGH animal facility. Then within a day if the animal looked healthy and eating well, we added 25% of 1% high cholesterol diet (1% HCD) containing 40% kcal fat, 1.25% (by weight) cholesterol and 0.5% (by weight) sodium cholate (D12109C, Research Diets). Gradually we increased 100% of their diet to 1% HCD during the first week of arrival. We kept daily dietary record of each mouse and its body weight. After four weeks on the 1% HCD, diabetes was induced by 5 consecutive day of intra-peritoneal injection of streptozotocin (STZ, 40 mg/kg, Sigma-Aldrich). Two weeks after the diabetic induction, the left common carotid artery was ligated below the bifurcation with 5-0 silk ligature (Ethicon) fewer than 2% Isoflurane anesthetic. The non-ligated right carotid serves as a negative control.

Atherosclerotic Plaques imaging with 3MBA-Au-144-NPs and XFCT

Before imaging of *in vivo* mice, a vial filled with 3MBA-Au-144-NPs (100 mg/mL consists of 2.9×10^{-8} moles/1.7×10^{16} particles) was imaged for XFCT side-by-side with 0.9% saline filled vial by a cone-beam micro-CT. Two weeks after carotid ligation, mice were injected 250 µl of 3MBA-Au-144-NPs intravenously (IV) through tail vein an hour before imaging with micro-CT for XFCT imaging. As a proof-of-concept, the XFCT was performed in a cone-beam micro-CT system (40 kV, 0.64 mA, Triumph, TriFoil Imaging, and Chatsworth, CA, USA) under 2% Isoflurane in the prone position, acquiring a single line integral at a time. Images were reconstructed using various filtered back-projection settings in the imaging software (Optimal Resolution, General Purpose, and Optimal Noise), at 177 µm resolution. Reconstructed images were exported as DICOMs using the Amira software (Zuse Institute Berlin, Germany and Thermo Fisher Scientific, Waltham, MA).

IMAGE ANALYSIS

The Region-of-Interest (ROI) statistics and 3D view of the XFCT images were analyzed with Materialise Mimics, a 3D medical image processing software.

STATISTICAL ANALYSES

A pairwise two-sample Student's t-test was performed to compare XRF signals between (1) vials filled with 3MBA-Au-144-NPs vs. 0.9% saline; (2) *in vivo* mice left carotid ligation vs. non-ligated right carotid arteries after 3MBA-Au-144-NPs IV injection. Weight and dose were not considered in the statistical analysis as we used all mice with same weight and 3MBA-Au-144-NPs doses. We presented all values as mean ± standard deviation. Statistical significance is considered at $p<0.05$.

RESULTS

Two distinctive L-shell energy peaks were observed at 10 KeV and 11.13 KeV for 3MBA-Au-144-NPs in the energy spectrum (Figure 4). K-shell fluorescence events vanished in the Compton scatter and characteristic background of the tungsten source due to the lead shielding for the SD and CdTe detectors. The distinctive L-shell fluorescence energy peaks of 3MBA-Au-144-NPs were useful characteristic feature for molecular imaging. We also observed a space missing at 12.5 KeV.

The XRF peaks in the spectra were processed into sonogram for the NPs and reconstructed with MLEM algorithm (Figure 5A).

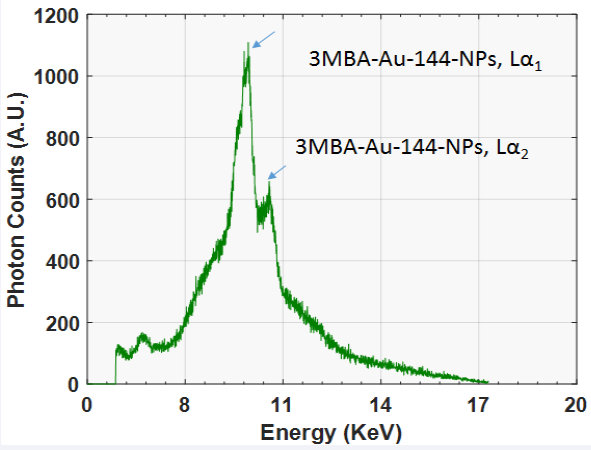

Figure 4 An XRF spectral fingerprint of 3MBA-Au- 144-NPs is exhibited at 10 KeV and 11.13 KeV excited with 320 KeV X-ray sources.

The distribution of the 3MBA-Au-144-NPs is clearly identified on the reconstructed image (Figure 5B). Reconstructed XFCT image from the generated sonogram was based on XRF peaks of 3MBA-Au-144-NPs in the acquired spectra. The signal intensity varied with different 3MBA-Au-144-NPs concentration distribution (correlated with the image intensity) of 0.85, 1.7, 3.4, and 17.0 mg/ml or 5%, 10%, 20%, and 100% (Figure 5C), respectively. The XRF intensity showed a highly linear response (R^2=0.999) with respect to different concentrations of 3MBA-Au-144-NPs (Figure 6). The XRF signal from 3MBA-Au-144-NPs was 1.67× higher (132.15 ± 26.30 vs. 78.87 ± 25.18) compared to 0.9% saline (Figure 7). The results are statistically significance (p=0.001). None of the five left carotid ligated mice showed any XRF signal at baseline before 3MBA-Au-144-NPs was IV injected in both 1D images as well as the volumetric render images (Figure 8). However, a strong XRF signal was detected at 2 mm below the ligation of the left carotid arteries where plaque developed below the bifurcation (Figure 9). 1D image (Figure 9A), the white light image (Figure 9B), and render volumetric images (Figure 9C-9D) of the mice left carotid artery showed similar results. Although, we observed high XRF signal in the aortic arch of the ligated mice after the 3MBA-Au-144-NPs injection in the 1D image, 3D render images we were not able to detect.

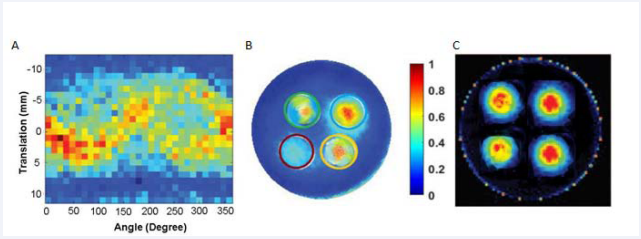

Figure 5 Reconstructed image of heart apex model with same volume of 3MBA-Au-144-NPs with different concentration. (A) Sinogram generated from XRF peaks of 3MBA-Au-144-NPs is exhibited at 10 KeV and 11.13 KeV excited with 320 KeV X-ray source; (B) reconstructed image using one iteration of maximum-likelihood expectation maximization (MLEM) algorithm (C) reconstructed XFCT image (the spatial position of different concentration of 3MBA-Au-144-NPs upper right: 0.1 mL NPs with 0 mL water, lower right: 0.1 mL NPs with 0.05 mL water, upper left: 0.1 mL NPs with 0.1 mL water, lower left: 0.1 mL NPs with 0.2 mL water) using 25 iteration of MLEM.

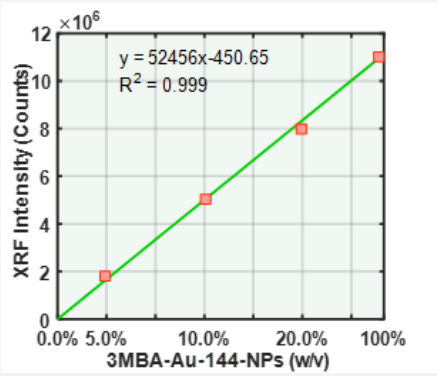

Figure 6 A highly linear relationship between the XRF intensity and the concentration of the 3MBA-Au-144- NPs (RR^2 =0.999).

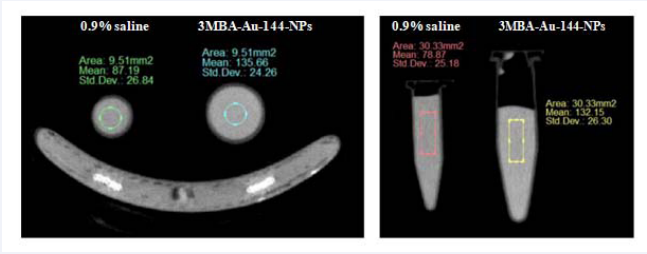

Figure 7 Side-by-side micro-CT images of 0.9% saline and 3MBA-Au-144-NPs. Contrast agent showed 1.67x higher signals compared to 0.9% saline at the highlighted region-of-interest (ROI) in both top and cross sectional view.

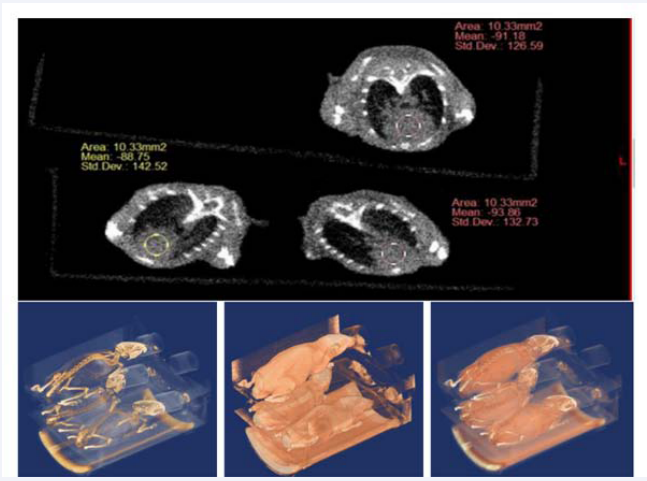

Figure 8 Baseline images of mice model. No higher XRF signals were detected in mice carotid ligation atherosclerotic model at baseline measurement before injecting 3MBA-Au-144-NPs.

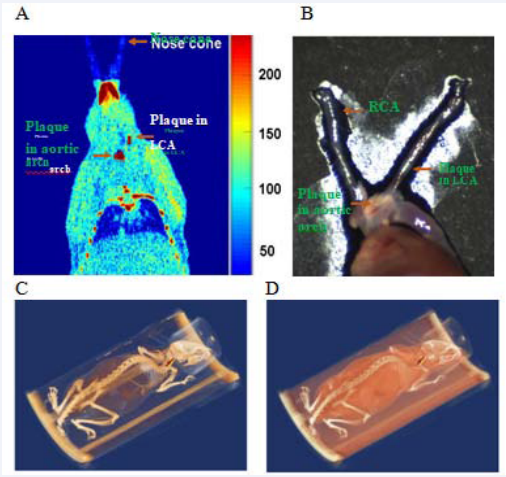

Figure 9 (A) Higher XRF signals were detected at the atherosclerotic plaque of a mouse ligated left carotid artery and aortic arch of the heart at 1 hour post 3MBA-Au-144-NPs injecting. (B) For secondary verification extracted heart with left and right carotid artery was imaged with an in-house near-infrared fluorescence imaging system confirmed similar results as with XFCT. (C-D) 3D volumetric render image at 1 hour post 3MBA-Au-144-NPs injecting.

DISCUSSIONS

The number of XRF counts produced signal is proportional to the concentration of 3MBA-Au-144-NPs that leads to accurate quantification of gold-based molecular contrast agent. However, the lower limit to detect spatial distribution of 3MBA-Au-144-NPs is a key factor for developing XFCT imaging strategy. It is important to improve the lower limit of detection while keeping the radiation dose as low as possible. Our experimental design showed low to moderate scattering inside the chambers of the apex model and its surrounding materials lead to narrow background noise in the energy spectrum. The signal to noise ratio (SNR) was relatively higher than other studies done by researchers in our research group [1,2]. However, SNR could be further improved by polarized and monochromatic X-ray source for irradiation of the 3MBA-Au-144-NPs [2,11]. Monochromatic beams produced with synchrotron sources are known to give higher contrast for k-shell XRF signal than clinically polychromatic X-ray sources [12]. Another limitation of this study is the long image acquisition time due to the beams was acquired sequentially. To overcome this limitation, in future we could perform parallel imaging by using an X-ray photon counting detector array and multiple simultaneous excitation pencil beams. In addition, we can improve this XFCT imaging by using cone beam geometry [13].

However, the ability of these novel 3MBA-Au-144-NPs based XRF imaging will provide co-localized microstructural and biological image information that could enhance our understanding and management of the coronary artery disease (CAD). Inflammatory cells, such as macrophage infiltration can be identified by the micro-CT system can now be further characterized *in vivo* in terms of molecular expression and activity by the use of 3MBA-Au-144-NPs. This new capability could allow researchers and doctors to gain access to coronary plaques which is still challenging due to their small size, motion, and obscuring signal from adjacent myocardium.

This XFCT system in conjunction with 3MBA-Au-144-NPs could provide diagnostic solution to identify individuals at higher risk by identifying culprit lesions in the coronary artery tree and initiate treatment to prevent the rupture of the plaques and infarction of the myocardium. This will enable early initiation of personalized therapy before irreversible damage occurs. Furthermore, this imaging modality has the potential to identify patients with acute MI that are at risk of enhanced remodeling, and to steer yet-to-be-defined therapies that stop this process early before heart failure occurs.

CONCLUSIONS

We have demonstrated that capability of XFCT to image spatial distribution and concentration of 3MBA-Au-144-NPs. Although, this proof of concept study may anticipate a long way to be a part of the clinically used imaging toolbox, it surely shows promises of non-invasive way to detect the 3MBA-Au-144-NPs to detect unstable atherosclerotic plaques in carotid arteries with a whole-body molecular imaging.

SUMMARY OF KEY POINTS

Question

Can XFCT be a suitable non-invasive molecular imaging tool to detect unstable plaques?

Pertinent findings

In a small cohort *in vivo* mice carotid atherosclerotic study, we have identified that XFCT in conjunction with a high-Z X-ray crystal nanoparticle can locate unstable plaques in carotid arteries with high sensitivity. We have also identified two L -shell energy peaks from the X-ray crystal due to characteristic augur electrons with missing K-shell fluorescence events in the Compton scatter and characteristic background of the tungsten source.

Implication for patient care

The transitional implication of this study will help detect the location of unstable plaques during the evaluation of the arterial wall before stent implantation by the interventional cardiologist.

AUTHOR CONTRIBUTIONS STATEMENT

Specific contribution of the authors (initials) is listed here. RTZ (PI): design and system development, experimental set up and conduct experiment, data and statistical analysis, manuscript writing, DV: experimental set up and conduct experiment, data analysis, review and writing manuscript; LX: review manuscript.

FINANCIAL SUPPORT

This study was partly support by the National Heart, Lung, and Blood Institute of the National Institutes of Health under award numbers R00HL127180.

DATA AVAILABILITY STATEMENT

All the generated data in this study were analyzed and included in this manuscript in form of Figures.

ACKNOWLEDGEMENT

The authors of these manuscripts are grateful to Dr. Roger Kornberg and Dr. Maia Azubel for providing the nanoparticles that was designed and synthesized in the Roger Kornberg's Laboratory at Stanford University School of Medicine.

REFERENCES

1. Yu Kuang, Guillem Pratx, Magdalena Bazalova, Bowen Meng, Jianguo Qian, Lei Xing. First demonstration of multiplexed X-ray fluorescence computed tomography (XFCT) imaging. IEEE Trans. Med Imag. 2013; 32: 262-267.

2. Yu Kuang, Guillem Pratx, Magdalena Bazalova, Jianguo Qian, Bowen Meng, Lei Xing. Development of XFCT imaging strategy for monitoring the spatial distribution of platinum-based chemo drugs: instrumentation and phantom validation. Med Phys. 2013; 40: 030701.

3. Maia Azubel, Roger D. Kornberg. Synthesis of Water-Soluble, Thiolate-Protected Gold Nanoparticles Uniform in Size. Nano Lett. 2016; 16: 3348-3351.

4. Magdalena Bazalova, Yu Kuang, Guillem Pratx, Lei Xing. Investigation of X-ray fluorescence computed tomography (XFCT) and K-edge imaging. IEEE Trans. Med Imag. 2012; 31: 1620-1627.

5. Seong-Kyun Cheong, Bernard L Jones, Arsalan K Siddiqi, Fang Liu, Nivedh Manohar, Sang Hyun Cho. X-ray fluorescence computed tomography (XFCT) imaging of gold nanoparticle-loaded objects using 110 kVp x-rays. Phys Med Biol. 2010; 55: 647-662.

6. Bernard L Jones, Sang Hyun Cho. The feasibility of polychromatic

cone-beam x-ray fluorescence computed tomography (XFCT) imaging of gold nanoparticle-loaded objects: a Monte Carlo study. Phys Med Biol. 2011; 56: 3719-3730.

7. Hisanori Kosuge, Sarah P Sherlock, Toshiro Kitagawa, Rajesh Dash, Joshua T Robinson, Hongjie Dai. Near infrared imaging and photothermal ablation of vascular inflammation using single-walled carbon nanotubes. J Am Heart Assoc. 2012.

8. Masahiro Terashima 1, Masaki Uchida, Hisanori Kosuge, Philip S Tsao, Mark J Young, Steven M Conolly, et al. Human ferritin cages for imaging vascular macrophages. Biomaterials. 2011; 32: 1430-1437.

9. Hisanori Kosuge, Sarah P. Sherlock, Toshiro Kitagawa, Masahiro Terashima, Joëlle K. Barral, Dwight G. Nishimura, et al. FeCo/Graphite Nanocrystals for Multi-Modality Imaging of Experimental Vascular Inflammation. Plos One 6. 2011.

10. Masaki Uchida, Hisanori Kosuge, Masahiro Terashima, Deborah A. Willits, Lars O. Liepold, Mark J. Young, et al. Protein cage nanoparticles bearing the LyP-1 peptide for enhanced imaging of macrophage-rich vascular lesions. ACS Nano. 2011; 5; 2493-2502.

11. Ali PA, Bennet C, el-Sharkawi AM, Hancock DA. Plane polarized x-ray fluorescence system for the in vivo measurement of platinum in head and neck tumours. Phys Med Biol. 1998; 43: 2337-2345.

12. K Ricketts, A Castoldi, C Guazzoni, C Ozkan, C Christodoulou, A P Gibson, G J Royle. A quantitative x-ray detection system for gold nanoparticle tumour biomarkers. Phys Med Biol. 2012; 57: 5543-5555.

13. Bernard L Jones, Nivedh Manohar, Francisco Reynoso, Andrew Karellas, Sang Hyun Cho. Experimental demonstration of benchtop x-ray fluorescence computed tomography (XFCT) of gold nanoparticle-loaded objects using lead- and tin-filtered polychromatic cone-beams. Phys Med Biol. 2012; 57: N457-467.

Cite this article

Zaman RT, Vernekhol D, Xing L (2020) Distinctive Energy Profile of Water-Soluble, Thiolate-Protected Gold Nanoparticles as Potential Molecular Marker for Vulnerable Plaque Detection with XFCT Imaging. J Radiol Radiat Ther 7(1): 1087.